Infrared Spectra of Metallacyclopropane, Insertion, and Dihydrido Complex Products in Reactions of Laser-Ablated Group 6 Metal Atoms with Ethylene Molecules

Han-Gook Cho and Lester Andrews*

Department of Chemistry, University of Incheon, 177 Dohwa-dong, Nam-ku, Incheon 402-749, South Korea, and Department of Chemistry, University of Virginia, P.O. Box 400319, Charlottesville, Virginia 22904-4319

Received: July 10, 2008; Revised Manuscript Received: September 25, 2008

Reactions of laser-ablated group 6 metal atoms with ethylene have been investigated. The insertion and dihydrido products ($MH-CHCH_2$ and $MH_2-C_2H_2$) are identified from reactions of W and Mo with ethylene isotopomers, whereas products in the Cr spectra are assigned to the insertion and metallacyclopropane ($M-C_2H_4$) complexes. Our experiments with CH_2CD_2 show that the dihydrido complex is formed by β-hydrogen transfer in the insertion complex because the MHD−CHCD isotopic product is favored. The present matrix infrared spectra and DFT computational results support the general trend that the higher oxidation-state complexes become more stable on going down the group 6 column. Unlike the cases of group 4 and 5 metals, binary metal hydride (MH_x) absorptions are not observed in the infrared spectra, suggesting that the H_2-elimination reactions of ethylene by group 6 metals are relatively slow, consistent with previous gas-phase reaction dynamics studies.

Introduction

Insertion into the C−H bond and the following rearrangement are key steps for numerous synthetic reactions and catalytic processes.[1,2] Particularly those processes initiated by transition-metal atoms have drawn much attention recently.[1,3] The simple metal complexes produced in reactions of metal atoms and simple organic compounds often show unique structures and photochemical properties including photoreversibility.[3,4] Reactions of ethylene with transition-metal atoms often result in elimination of H_2 and have been the subject of many reaction dynamics studies.[5−7] The details of the reaction path have been carefully examined theoretically as well as experimentally.[5−10] A series of studies has been performed for the reactions of hydrocarbons and the second-row transition metals.[10,11]

It is generally accepted that H_2-elimination by transition-metal atom proceeds in the order of M + ethylene → π-complex → metallacyclopropane → insertion product → dihydrido complex → $M-C_2H_2 + H_2$.[9] The early transition-metal atom first forms a weak π-complex with ethylene, which then converts into a strongly bound complex (metallacyclopropane). It in turn rearranges to an insertion product ($MH-CHCH_2$) and later to a dihydrido product ($MH_2-C_2H_2$). H_2-elimination is believed to occur from the dihydrido complex, leaving a metal−acetylene complex. Carroll et al. measured the reaction rate coefficients of several hydrocarbons including ethylene with early second-row transition metals and their neutral diatomic oxides.[11] They reported that the group 4 metal is most reactive among the second-row early transition metals.

While the reactions of group 4 metals with ethylene have been studied most,[4,5,9] the H_2-elimination reactions of group 3 and 5 metals are also reported to be fairly efficient.[6,7] Davis et al. proposed that the single most stable reaction intermediates in the Y and Nb reactions are the insertion and dihydrido complexes, respectively.[6,7] The primary reaction intermediates of groups 4 and 5 ($MH-C_2H_3$ and $MH_2-C_2H_2$ for group 4 metals and $MH_2-C_2H_2$ for group 5 metals) were later identified from the matrix IR spectra.[12,13] While the observed intermediates confirm the reaction path suggested by the previous studies and give more insight into the reaction mechanism, the trihydrido complex (MH_3-CCH), previously unexpected, is also identified from the Zr and Hf reactions.[12]

In this study, we report matrix IR spectra from reactions of laser-ablated group 6 metal atoms with ethylene isotopomers. The reaction products from C−H insertion and following rearrangement are identified, and the primary products vary on going down the group 6 column. Unlike the cases of group 4 and 5 metals, no metal hydride absorptions are observed, suggesting that H_2-elimination by group 6 metals is considerably slower. In addition, DFT computations reproduce the stability of the products and their vibrational characteristics.

Experimental and Computational Methods

Laser-ablated group 6 metal atoms (Johnson-Matthey) were reacted with C_2H_4, C_2D_4, $^{13}C_2H_4$ (Cambridge Isotope Laboratories, 99%), and CH_2CD_2 (MSD Isotopes) in excess argon during condensation at 10 K using a closed-cycle refrigerator (Air Products Displex). These methods have been described in detail elsewhere.[3,14] Reagent gas mixtures ranged 0.5−1.0% in argon. After reaction, infrared spectra were recorded at a resolution of 0.5 cm^{-1} using a Nicolet 550 spectrometer with an MCT-B detector. Samples were later irradiated for 20 min periods by a mercury arc street lamp (175 W) with the globe removed and a combination of long wavelength pass optical filters, and subsequently annealed to allow further reagent diffusion.[14]

To support the assignment of new experimental frequencies, and to correlate with our group 4 and 5 investigations,[12,13] similar density functional theory (DFT) calculations were carried out using the Gaussian 03 package,[15] B3LYP density functional,[16] 6-311++G(3df,3pd) basis sets for C, H, Cr,[17] and SDD pseudopotential and basis set[18] for Mo and W to provide a consistent set of vibrational frequencies for the reaction products. Geometries were fully relaxed during optimization, and the

* Corresponding author. E-mail: lsa@virginia.edu.

10.1021/jp806110h CCC: $40.75
Published on Web 11/01/2008

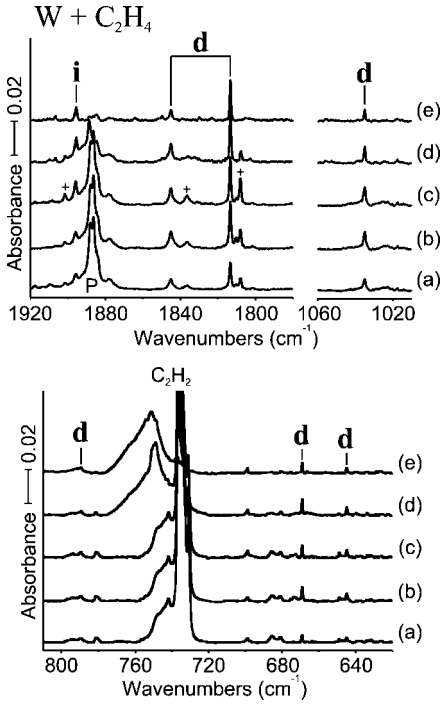

Figure 1. IR spectra in the regions of 1920−1780, 1060−1010, and 810−620 cm^{-1} for laser-ablated W atoms codeposited with C_2H_4 in excess argon at 10 K and their variation. (a) W + 0.5% C_2H_4 in Ar codeposited for 1 h. (b) As (a) after photolysis with $\lambda > 420$ nm. (c) As (b) after photolysis with $240 < \lambda < 380$ nm. (d) As (c) after annealing to 36 K. (e) As (d) after annealing to 44 K. **i** and **d** denote the product absorption groups, and + designates a matrix site absorption of the primary species.

optimized geometry was confirmed by vibrational analysis. BPW91[19] calculations were also done to complement the B3LYP results. The vibrational frequencies were calculated analytically, and the zero-point energy is included in the calculation of binding energies. Previous investigations have shown that DFT calculated harmonic frequencies are usually slightly higher than observed frequencies,[3,14,20] depending on the mode anharmonicity, and they provide useful predictions for infrared spectra of new molecules.

Results and Discussion

Reactions of laser-ablated group 6 metal atoms with ethylene isotopomers were carried out, and the matrix infrared spectra of new products will be compared to frequencies calculated by density functional theory.

W + C_2H_4. Figure 1 shows the C_2H_4 spectra in the C−H stretching, HCCH in-plane bending, and low frequency regions. Two sets of product absorptions marked "**d**" and "**i**" (**d** for dihydrido and **i** for insertion products) are observed on the basis of the intensity variations upon photolysis and annealing. The **d** absorptions almost double on visible ($\lambda > 420$ nm) irradiation, remain almost the same on UV ($240 < \lambda < 380$ nm) irradiation, and gradually decrease in the process of annealing. In contrast, the **i** absorption increases only slightly on visible photolysis, but almost doubles on UV irradiation. The observed frequencies are listed in Table 1 and compared to DFT computed frequencies in Tables 2 and 3.

The **d** absorptions in the W−H stretching region at 1845.7 and 1813.3 cm^{-1} with about 1:2 intensity ratio have their D counterparts at 1318.9 and 1302.5 cm^{-1} (H/D ratios of 1.399 and 1.392) as shown in Figure 2 and show negligible ^{13}C shifts as listed in Tables 1 and 2. They are also compared to the hydrogen stretching frequencies of WH_x (1852.6, 1816.8, and 1878.6 cm^{-1} for WH, WH_2, and WH_3, respectively) and the deuterium counterparts (1327.6 and 1344.3 cm^{-1} for WD and WD_3).[21] It is also notable that the tungsten hydride absorptions are not observed in this study unlike the previous matrix studies of group 4 and 5 metals, where metal hydride absorptions, particularly the dihydrides, are among the major product absorptions.[12,13] The two strong W−H stretching absorptions indicate that a primary reaction product with a WH_2 group is generated. Most probably this is a dihydrido complex ($WH_2-C_2H_2$) similar to the groups 4 and 5 product.[4,12,13] These bands are due to symmetric and antisymmetric W−H stretching modes, as the slightly lower H/D ratio and stronger absorption are appropriate for the antisymmetric motion.

The **d** absorption at 1035.0 cm^{-1} has its D and ^{13}C counterparts at 909.9 and 1016.1 cm^{-1} (H/D and 12/13 ratios of 1.137 and 1.019) and is assigned to the HCCH in-plane bending mode of $WH_2-C_2H_2$ on the basis of the frequency, isotopic shifts, and agreements with DFT values. A weak **d** absorption at 789.6 cm^{-1} has its D and ^{13}C counterparts at 582.3 and 784.2 cm^{-1} (H/D and 12/13 ratios of 1.356 and 1.007) and is assigned to the WH_2 scissoring mode on the basis of the large D and small ^{13}C shifts. The **d** absorption at 669.1 cm^{-1} is designated to the HCCH out-of-plane bending mode with the D and ^{13}C counterparts at 514.9 and 666.4 cm^{-1} (H/D and ^{13}C ratios of 1.299 and 1.004), due to the large D, small ^{13}C shifts, and agreement with DFT values. Another **d** absorption at 644.7 cm^{-1} has its D and ^{13}C counterparts at 545.5 and 631.5 cm^{-1} (H/D and 12/13 ratios of 1.182 and 1.021) and is assigned to the $W-C_2$ stretching mode on the basis of the frequency and sizable ^{13}C shift. The six observed frequencies are in the range of 0.956−0.998 times the B3LYP values as shown in Table 2, and the observed band absorbances are in good agreement with the relative computed infrared intensities (the symmetric W−H band is slightly broader than the antisymmetric counterpart). Note that the computed (B3LYP) harmonic H/D ratios for the

TABLE 1: Frequencies of Product Absorptions Observed from Reactions of Ethylene with W in Excess Argon[a]

	C_2H_4	C_2D_4	$^{13}C_2H_4$	CH_2CD_2	description
d	**1845.7**, 1836.5	**1318.9**, 1313.5	**1845.7**, 1836.6	1845.2, **1828.7**, 1821.4, 1813.0	A_1 WH_2 sym str.
	1813.3, 1808.0	**1302.5**, 1298.9	**1813.3**, 1807.9	1318.8, **1311.7**, 1302.5	B_1 WH_2 str.
	1035.0	909.9	1016.1	**977.2**, 975.0	B_2 HCCH IP bend
	789.6	582.3	784.2	694.9	A_1 WH_2 scis.
	669.1	514.9	666.4	568.0	B_1 HCCH OOP bend
	648.8, **644.7**	548.6, **545.5**	635.0, **631.5**		B_2 WC_2 str.
i	1901.6, **1895.7**	1363.9, **1360.6**	1901.2, **1895.8**	1901.1, **1895.2**, 1361.0	W−H str.
	578.2				C−W str.

[a] All frequencies are in cm^{-1}. Stronger absorptions in a set are bold. Description gives major coordinate. **d** and **i** stand for dihydrido and insertion products, respectively.

TABLE 2: Observed and Calculated Frequencies of the Fundamental Bands of $WH_2-C_2H_2$ in Its Ground $^3A_2$ State[a]

	$WH_2-C_2H_2$				$WD_2-C_2D_2$				$WH_2-{}^{13}C_2H_2$				WHD−C_2HD			
description	obs.[b]	BPW91[c]	B3LYP[d]	int.[d]	obs.[b]	BPW91[c]	B3LYP[d]	int.[d]	obs.[b]	BPW91[c]	B3LYP[d]	int.[d]	obs.[b]	BPW91[c]	B3LYP[d]	int.[d]
A_1 CH str.		3134.8	3202.0	1		2361.2	2411.5	0		3121.7	3188.6	1		3119.9	3187.1	2
A_1 WH_2 str.	1845.7	1864.1	1896.0	240	1318.9	1320.0	1342.7	119	1845.7	1864.1	1896.0	239	1828.7	1852.4	1883.4	257
A_1 C═C str.		1477.7	1517.4	14		1407.2	1445.4	15		1424.1	1462.4	14		1441.6	1480.6	14
A_1 HCCH IP bend		858.5	877.7	0		677.7	683.8	5		855.0	874.7	1		749.2	761.1	8
A_1 WH_2 scis.	789.6	791.2	791.1	35	582.3	578.3	586.4	16	784.2	789.8	789.2	35	694.9	704.2	706.9	27
A_1 WC_2 str.		566.7	569.5	1		488.7	490.6	1		550.7	553.4	1		524.9	531.3	9
A_2 HCCH OOP bend		873.8	921.6	0		706.5	744.9	0		863.9	911.2	0		818.8	862.6	8
A_2 WH_2 twist		445.3	443.6	0		333.8	332.2	0		442.2	440.6	0		414.9	420.3	10
B_1 WH_2 str.	1813.3	1841.7	1871.8	279	1302.5	1309.3	1330.8	142	1813.3	1841.7	1871.8	279	1311.7	1315.7	1337.8	133
B_1 HCCH OOP bend	669.1	670.6	700.2	50	514.9	506.5	529.2	26	666.4	667.1	696.5	50	568.0	561.8	586.4	29
B_1 WH_2 rock		392.3	397.8	1		284.9	288.5	1		391.6	397.1	1		319.7	323.8	2
B_2 CH str.		3104.0	3171.2	2		2281.9	2331.4	1		3094.8	3161.7	2		2322.1	2372.1	1
B_2 HCCH IP bend	1035.0	1017.8	1062.6	61	909.9	885.9	919.3	27	1016.1	999.6	1044.1	62	977.2	977.8	1017.4	45
B_2 WC_2 str.	644.7	642.3	646.5	29	545.5	540.4	547.3	26	631.5	627.4	631.1	27		589.6	593.7	20
B_2 WH_2 wag.		380.2	401.9	34		272.9	288.4	18		379.6	401.3	34		299.0	310.6	14

[a] Frequencies and intensities are in cm^{-1} and km/mol. [b] Observed in an argon matrix. [c] Frequencies computed with BPW91/6-311++G(3df,3pd). [d] Frequencies and intensities computed with B3LYP/6-311++G(3df, 3pd). SDD core potential and basis set are used for W. $WH_2-C_2H_2$ has a C_{2v} structure.

TABLE 3: Observed and Calculated Frequencies of the Fundamental Bands of $WH-CHCH_2$ in Its Ground ^5A State[a]

	WH−CH_2CH				WD−CD_2CD				WH−$^{13}CH_2{}^{13}$CH			
description	obs.[b]	BPW91[c]	B3LYP[d]	int.[d]	obs.[b]	BPW91[c]	B3LYP[d]	int.[d]	obs.[b]	BPW91[c]	B3LYP[d]	int.[d]
CH_2 as. str.		3098.5	3155.9	13		2305.3	2348.6	5		3086.1	3143.2	14
C−H str.		3027.7	3087.2	7		2232.0	2274.1	1		3021.2	3080.7	8
CH_2 s. str.		3013.8	3069.7	9		2192.8	2236.2	5		3005.6	3061.1	9
W−H str.	1895.7	1902.1	1912.1	189	1360.6	1349.3	1356.4	96	1895.8	1902.1	1912.1	189
C═C str.		1511.7	1569.1	7		1418.1	1470.0	8		1481.2	1537.7	6
CH_2 scis.		1348.8	1396.8	14		1029.7	1068.1	7		1321.7	1368.6	14
HCCH IP s. bend		1207.2	1256.8	9		972.0	1007.1	3		1192.3	1241.6	9
HCCH OOP bend		947.8	999.3	17		720.0	767.2	1		944.6	995.9	18
HCCH IP as. bend		914.3	958.5	6		669.3	701.4	5		910.7	954.6	6
CH_2 wag		878.2	937.6	29		687.3	724.7	25		868.2	927.3	28
C−W str.	578.2	585.4	585.2	42		497.7	495.9	21		576.9	577.0	43
CWH bend		469.1	467.1	5		372.8	374.6	8		460.7	458.2	4
CH_2 twist		366.1	377.2	18		282.0	289.4	11		362.8	374.0	18
WH OOP bend		117.7	133.1	21		94.8	99.6	13		115.0	131.2	19
CCW bend		135.5	145.6	19		106.4	123.3	10		134.9	143.7	20

[a] Frequencies and intensities are in cm^{-1} and km/mol. [b] Observed in an argon matrix. [c] Frequencies computed with BPW91/6-311++G(3df,3pd). [d] Frequencies and intensities computed with B3LYP/6-311++G(3df, 3pd). SDD core potential and basis set are used for W. $WH-CHCH_2$ has a C_1 structure.

TABLE 4: Frequencies of Product Absorptions Observed from Reactions of Ethylene with Mo in Excess Argon[a]

	C_2H_4	C_2D_4	$^{13}C_2H_4$	CH_2CD_2	description
d	1761.7, **1753.9**	**1255.7**, 1249.8	1761.6, **1754.0**	**1740.7**, 1733.6, 1728.3	A_1 MoH_2 sym str.
	1728.6, 1723.2	**1247.5**, 1243.9	**1728.6**, 1723.3	1255.7, 1252.7, 1247.7, 1243.9	B_1 MoH_2 str.
	1477.4				A_1 C═C str.
	997.9	874.1	980.0	957.2	B_2 HCCH IP bend
	805.4	575.6	805.2		A_1 MoH_2 scis.
	687.4	505.8	683.7		B_1 HCCH OOP bend
	611.8	520.3, **517.1**	600.0		B_2 MoC_2 str.
i	**1790.8**, 1787.0	1274.6	**1790.8**, 1787.0	1790.5, 1274.6	Mo−H str.
	535.3				C−Mo str.

[a] All frequencies are in cm^{-1}. Stronger absorptions in a set are bold. Description gives major coordinate. **d** and **i** stand for dihydrido and insertion products, respectively.

symmetric and antisymmetric W−H stretching modes, 1.412 and 1.406, have the same relationship as the above observed (anharmonic) values. In summary, the excellent agreement between the observed matrix and the DFT calculated frequencies for the six product absorptions with the highest infrared intensities substantiates the identification of $WH_2-C_2H_2$ in the product spectrum.

The **i** absorption at 1895.7 cm^{-1} shows a D shift of −535.1 cm^{-1} (H/D ratio of 1.393) and essentially no ^{13}C shift. The W−H stretching absorption on the blue side of the WH_2 stretching absorptions of $WH_2-C_2H_2$ is assigned to the insertion complex ($WH-CHCH_2$) on the basis of the good agreement with the DFT values. The observed frequency and D shift are compared to the BPW91 and B3LYP calculated frequencies of

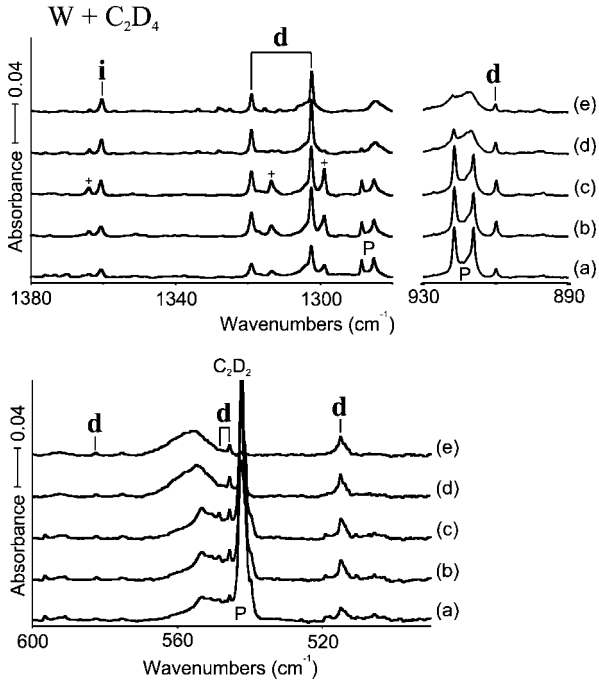

Figure 2. IR spectra in the regions of 1380−1280, 930−890, and 600−490 cm^{-1} for laser-ablated W atoms codeposited with C_2D_4 in excess argon at 10 K and their variation. (a) W + 0.5% C_2D_4 in Ar codeposited for 1 h. (b) As (a) after broadband photolysis with $\lambda >$ 420 nm. (c) As (b) after photolysis with 240 $< \lambda <$ 380 nm. (d) As (c) after annealing to 36 K. (e) As (d) after annealing to 44 K. **i** and **d** denote the product absorption groups, and + designates a site absorption of the primary species.

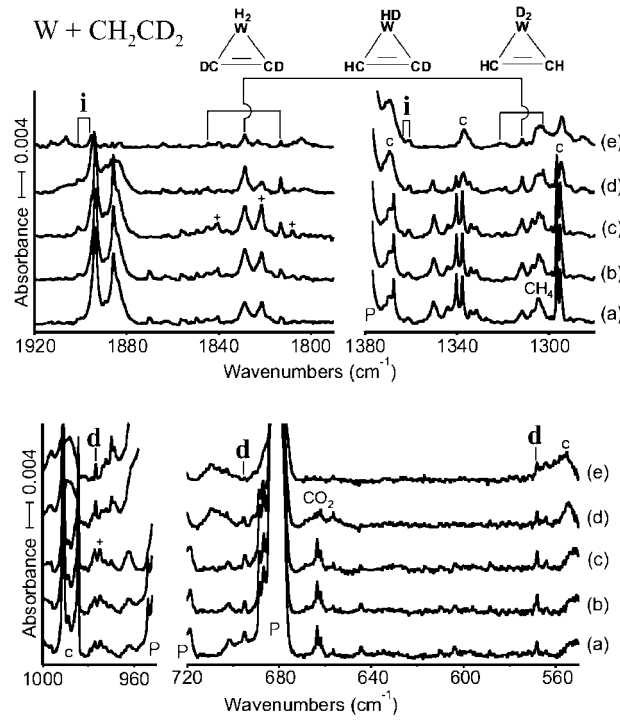

Figure 3. IR spectra in the regions of 1920−1790, 1380−1280, 1000−950, and 720−550 cm^{-1} for laser-ablated W atoms codeposited with CH_2CD_2 in excess argon at 10 K and their variation. (a) W + 1.0% CH_2CD_2 in Ar codeposited for 1 h. (b) As (a) after broadband photolysis with $\lambda >$ 420 nm. (c) As (b) after photolysis with 240 $< \lambda <$ 380 nm. (d) As (c) after annealing to 36 K. (e) As (d) after annealing to 44 K. **i** and **d** denote the product absorption groups. The dihydrido products responsible for the W−H stretching absorptions are also shown. c stands for common feature, and + designates a site absorption.

1902.1 and 1912.1 cm^{-1} and the D shifts of −552.8 and −555.7 cm^{-1} as shown in Table 3. The $WH-CHCH_2$(Q) and $WH_2-C_2H_2$(T) products are 35 and 53 kcal/mol more stable than the reactants ($^5W + C_2H_4$) (here Q denotes quintet and T triplet electronic states). The other vibrational bands of the insertion product are expected to be much weaker as shown in Table 3. However, the weak **i** absorption observed at 578.2 cm^{-1} (not shown) is designated as the C−W stretching mode without the D and ^{13}C counterparts.

Figure 3 shows the product absorptions from W reaction with CH_2CD_2. The W−H stretching absorption of WHD−CHCD at 1828.7 cm^{-1} is observed at the middle of the WH_2 stretching absorptions of $WH_2-C_2D_2$ at 1845.2 and 1813.0 cm^{-1} (Table 4). The W−D stretching absorption of WHD−CHCD at 1311.7 cm^{-1} is also observed at the middle of WD_2 stretching absorptions of the $WD_2-C_2H_2$ at 1318.8 and 1302.5 cm^{-1}. Observation of decoupled W−H and W−D stretching absorptions reconfirms formation of the dihydrido complex with two equivalent H atoms. The formation of a small amount of $WH_2-C_2D_2$ and $WD_2-C_2H_2$ along with stronger WHD−CHCD bands also suggests that additional scrambling of hydrogen atoms occurs between the carbon and metal atoms in the excited species formed initially during reaction of laser-ablated W atoms, due to the excess reagent energy. The **i** W−H and W−D stretching absorptions show essentially no frequency shifts, indicating that they originate from an unperturbed hydrogen stretching mode of $WH-CHCH_2$.

Mo + C_2H_4. The product absorptions from Mo reaction with ethylene isotopomers and their variations are illustrated in Figures 4−6. Parallel to the W case, two sets of product absorptions marked "**d**" and "**i**" are observed. The **d** absorptions double on visible irradiation, while the **i** absorption increases about 50%. The **d** absorptions increase only slightly on UV photolysis, but the **i** absorption increases more than 100%. The **d** absorptions gradually decrease in the process of annealing, whereas the **i** absorption first sharpens and later slowly decreases. The Mo spectra are in general similar to the W spectra (Figures 1−3) described above.

The **d** absorptions at 1753.9 and 1728.6 cm^{-1} with about 1:2 intensity ratio show D shifts of −498.2 and −481.2 cm^{-1} (H/D ratios of 1.397 and 1.386) and negligible ^{13}C shifts. They are also compared to 1691.6, 1718.7, and 1812.1 cm^{-1} bands for MoH, MoH_2, and MoH_4 and to 1218.4, 1234.2, and 1301.9 cm^{-1} for MoD, MoD_2, and MoD_4.[22] The Mo−H stretching frequencies with 1:2 intensity ratio strongly suggest that a primary product with a MoH_2 group, most probably $MoH_2-C_2H_2$, is generated in the reaction of atomic Mo with ethylene, parallel to the W case. No molybdenum hydride absorptions are observed, indicating that H_2-elimination of ethylene by Mo is relatively slow, similar to the W case.

The **d** absorption at 997.9 cm^{-1} has its D and ^{13}C counterparts at 874.1 and 980.0 cm^{-1} (H/D and 12/13 ratios of 1.142 and 1.018) and is assigned to the HCCH in-plane bending mode of $MoH_2-C_2H_2$ on the basis of the frequency and isotopic shifts. The **d** absorption at 805.4 cm^{-1} has its D and ^{13}C counterparts at 575.6 and 805.2 cm^{-1} (H/D and 12/13 ratios of 1.399 and 1.000) and is designated to the MoH_2 scissoring mode on the basis of the large D and negligible ^{13}C shifts. The **d** absorption at 687.4 cm^{-1} shows D and ^{13}C shifts of −181.6 and −3.7 cm^{-1} (H/D and 12/13 ratios of 1.359 and 1.005) and is assigned to the HCCH out-of-plane bending mode. Another **d** absorption at 611.8 cm^{-1}, which has its D and ^{13}C counterpart at 517.1 and 600.0 cm^{-1} (H/D and 12/13 ratios of 1.183 and 1.020), is assigned to the MoC_2 stretching mode. The weak **d** absorption

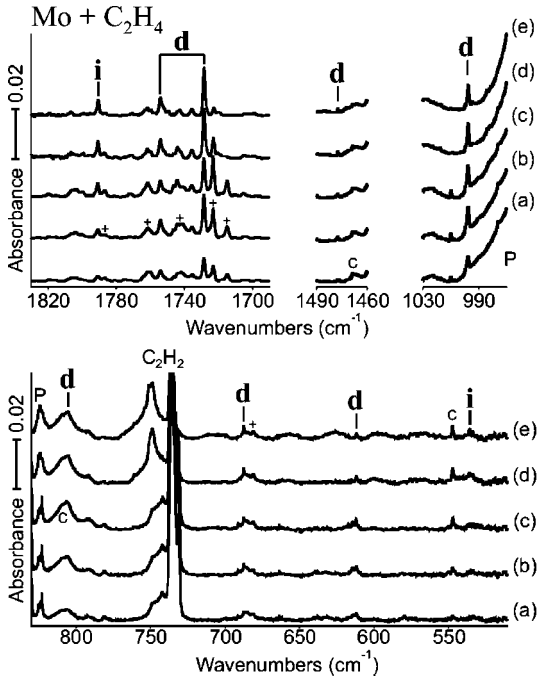

Figure 4. IR spectra in the regions of 1830−1690, 1490−1460, 1030−970, and 830−510 cm^{-1} for laser-ablated Mo atoms codeposited with C_2H_4 in excess argon at 10 K and their variation. (a) Mo + 0.5% C_2H_4 in Ar codeposited for 1 h. (b) As (a) after broadband photolysis with $\lambda > 420$ nm. (c) As (b) after photolysis with $240 < \lambda < 380$ nm. (d) As (c) after annealing to 36 K. (e) As (d) after annealing to 44 K. **i** and **d** denote the product absorption groups. + designates a site absorption. c and P stand for common feature and precursor band, respectively.

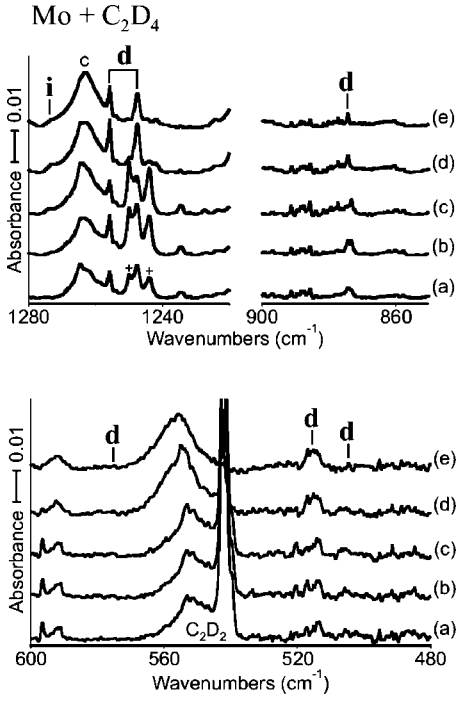

Figure 5. IR spectra in the regions of 1280−1220, 900−850, and 600−480 cm^{-1} for laser-ablated Mo atoms codeposited with C_2D_4 in excess argon at 10 K and their variation. (a) Mo + 0.5% C_2D_4 in Ar codeposited for 1 h. (b) As (a) after broadband photolysis with $\lambda > 420$ nm. (c) As (b) after photolysis with $240 < \lambda < 380$ nm. (d) As (c) after annealing to 36 K. (e) As (d) after annealing to 44 K. **i** and **d** denote the product absorption groups. + indicates a site absorption. C stands for common feature.

at 1477.4 cm^{-1} is tentatively assigned to the C−C stretching mode without observation of the D and ^{13}C counterparts. The

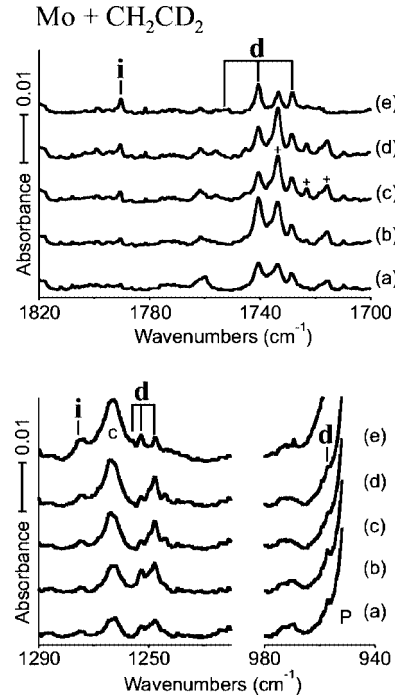

Figure 6. IR spectra in the regions of 1820−1700, 1290−1220, and 980−940 cm^{-1} for laser-ablated Mo atoms codeposited with CH_2CD_2 in excess argon at 10 K and their variation. (a) Mo + 1.0% CH_2CD_2 in Ar codeposited for 1 h. (b) As (a) after photolysis with $\lambda > 420$ nm. (c) As (b) after photolysis with $240 < \lambda < 380$ nm. (d) As (c) after annealing to 36 K. (e) As (d) after annealing to 44 K. **i** and **d** denote the product absorption groups. + indicates a site absorption. C stands for common feature.

observed frequencies are in the range of 0.950−1.000 of the B3LYP frequencies as shown in Table 5.

The **i** absorption at 1790.8 cm^{-1} has its D counterparts at 1274.6 cm^{-1} (H/D ratio of 1.405) in a region heavily overlapped by a common feature centered at 1262.2 cm^{-1}, but shows a negligible ^{13}C shift. Being consistent with the W case described above, the **i** absorption is assigned to the W−H stretching mode of the insertion product ($MoH-CHCH_2$). The observed Mo−H and Mo−D stretching frequencies are compared to the B3LYP frequencies of 1810.0 and 1286.9 cm^{-1} (H/D ratio of 1.406). The weak **i** absorption at 535.3 cm^{-1} is tentatively assigned to the C−Mo stretching mode without observation of the D and ^{13}C counterparts. The $MoH-CHCH_2$ and $MoH_2-C_2H_2$ molecules are energetically comparable, 10 and 15 kcal/mol more stable than the reactants ($^7Mo + C_2H_4$) (Table 6).

Figure 6 shows the product spectra from reaction of Mo and CH_2D_2. The **d** Mo−H stretching absorption of MoHD−CHCD is observed at 1740.7 cm^{-1} (along with a site absorption at 1733.6 cm^{-1}) in the middle of the MoH_2 absorptions of $MoH_2-C_2D_2$ at 1754.0 and 1728.3 cm^{-1}. The Mo−D stretching absorption is observed at 1252.7 cm^{-1} (with a site absorption at 1247.7 cm^{-1}). The decoupled Mo−H and Mo−D absorptions in the CH_2CD_2 spectra again confirm formation of the dihydrido Mo product. Essentially no frequency shift is observed for the **i** Mo−H and Mo−D stretching absorptions, corroborating the fact that they arise from an unperturbed hydrogen stretching mode of $MoH-CHCH_2$.

Cr + C_2H_4. Shown in Figure 7 are the product spectra from reactions of Cr with ethylene isotopomers. Two sets of product absorptions marked "**i**" and "**a**" (**i** and **a** for insertion and metallacyclopropane complex) are observed. Both **i** and **a** absorptions remain unchanged on visible irradiation, but they

TABLE 5: Observed and Calculated Frequencies of the Fundamental Bands of $MoH_2-C_2H_2$ in Its Ground $^3A_2$ State[a]

	$MoH_2-C_2H_2$				$MoD_2-C_2D_2$				$MoH_2-{}^{13}C_2H_2$				$MoHD-C_2HD$			
description	obs.[b]	BPW91[c]	B3LYP[d]	int.[d]	obs.[b]	BPW91[c]	B3LYP[d]	int.[d]	obs.[b]	BPW91[c]	B3LYP[d]	int.[d]	obs.[b]	BPW91[c]	B3LYP[d]	int.[d]
A_1 CH str.		3144.2	3213.7	0		2373.7	2426.1	0		3130.7	3199.9	1		3127.6	3197.1	0
A_1 MoH_2 str.	1753.9	1808.1	1833.6	267.0	1255.7	1281.5	1299.8	137	1754.0	1808.0	1833.6	270	1740.7	1801.4	1825.7	302
A_1 C═C str.	1477.4	1507.7	1547.7	17		1431.1	1468.7	16	covered	1453.4	1492.0	16	covered	1468.3	1507.1	16
A_1 HCCH IP bend		844.9	856.0	0		679.2	679.9	8		840.6	852.5	0		749.4	751.9	11
A_1 MoH_2 scis.	805.4	813.3	816.1	45	45	583.1	590.6	18	805.2	813.2	815.5	44		709.2	716.8	24
A_1 MoC_2 str.		572.9	573.1	1			499.3	0		558.1	558.1	1		519.5	524.6	22
A_2 HCCH OOP bend		860.1	903.7	0		696.5	731.7	0		850.2	893.2	0		808.4	848.6	7
A_2 MoH_2 twist		438.1	438.6	0			327.4	0		435.4	435.8	0		403.7	408.4	19
B_1 MoH_2 str.	1728.6	1796.1	1819.2	339	339	1282.2	1298.9	173	1728.6	1796.1	1819.2	339	1252.7	1283.2	1300.6	159
B_1 HCCH OOP bend	687.4	675.8	705.4	40	505.8	512.0	534.7	20	683.7	672.1	701.5	40		577.5	591.0	23
B_1 MoH_2 rock		399.0	401.8	1		289.3	291.3	1		398.4	401.3	1		325.2	327.3	1
B_2 CH str.		3109.8	3179.2	0		2285.0	2336.1	0		3100.6	3169.8	0		2330.1	2382.0	1
B_2 HCCH IP bend	997.9	990.2	1031.8	71	874.1	861.7	893.3	30	980.0	972.5	1013.7	72	957.2	951.8	988.3	52
B_2 MoC_2 str.	611.8	611.4	611.8	39	517.1	516.5	519.7	35	600.0	597.3	597.4	36		564.7	575.0	16
B_2 MoH_2 wag.		350.7	368.9	75		252.7	265.7	38		350.4	368.6	74		279.3	290.9	36

[a] Frequencies and intensities are in cm^{-1} and km/mol. [b] Observed in an argon matrix. [c] Frequencies computed with BPW91/6-311++G(3df,3pd). [d] Frequencies and intensities computed with B3LYP/6-311++G(3df, 3pd). SDD core potential and basis set are used for Mo. $MoH_2-C_2H_2$ has a C_{2v} structure.

TABLE 6: Observed and Calculated Frequencies of the Fundamental Bands of MoH−CHCH$_2$ in Its Ground ^{5}A State[a]

	MoH−CHCH$_2$				MoD−CDCD$_2$				MoH−^{13}CH^{13}CH$_2$			
description	obs.[b]	BPW91[c]	B3LYP[d]	int.[d]	obs.[b]	BPW91[c]	B3LYP[d]	int.[d]	obs.[b]	BPW91[c]	B3LYP[d]	int.[d]
CH$_2$ as. str.		3088.2	3144.7	16		2297.2	2339.7	5		3075.9	3132.1	17
C−H str.		3029.1	3085.6	3		2238.9	2280.6	1		3020.1	3076.8	4
CH$_2$ s. str.		3014.8	3073.2	14		2189.7	2233.1	5		3008.9	3066.8	13
Mo−H str.	1790.8	1809.4	1810.0	258	1274.6	1286.4	1286.9	132	1790.8	1809.3	1810.0	258
C═C str.		1521.1	1578.5	5		1433.9	1486.2	6		1487.2	1543.5	4
CH$_2$ scis.		1355.7	1403.7	13		1025.7	1064.2	7		1331.3	1378.2	13
HCCH IP s. bend		1197.3	1246.8	19		967.5	1002.6	5		1182.4	1231.6	19
HCCH OOP bend		951.6	1003.3	16		723.3	769.5	1		948.6	1000.0	17
HCCH IP as. bend		906.5	950.5	11		663.1	694.6	7		903.1	946.7	10
CH$_2$ wag		885.1	942.1	30		691.5	728.4	25		875.0	931.9	28
C−Mo str.	535.3	550.4	546.1	85		482.4	479.0	41		541.2	536.9	87
CMoH bend		456.0	454.3	18		356.1	357.3	20		449.6	447.6	14
CH$_2$ twist		357.8	363.8	25		274.8	227.7	16		354.7	360.9	25
CCMo bend		127.8	141.9	20		108.1	122.3	15		125.6	139.0	20
MoH OOP bend		100.1	101.0	49		75.0	74.9	25		99.2	100.4	49

[a] Frequencies and intensities are in cm^{-1} and km/mol. [b] Observed in an argon matrix. [c] Frequencies computed with BPW91/6-311++G(3df,3pd). [d] Frequencies and intensities computed with B3LYP/6-311++G(3df, 3pd). SDD core potential and basis set are used for Mo. MoH−CHCH$_2$ has a C_1 structure.

quadruple and decrease about 50% on UV irradiation and annealing, respectively. Fewer product absorptions are observed than in the W and Mo spectra in Figures 1−6. The observed frequencies are listed in Table 7 and compared to the DFT frequencies in Tables 8 and 9.

The **i** absorptions at 1635.5 and 1628.8 cm^{-1}, believed split by the matrix, have their D counterparts at 1179.6 and 1173.8 cm^{-1} (H/D ratios of 1.386 and 1.387) and show negligible ^{13}C shifts. The observed Cr−H stretching frequencies can be compared to 1603.3 cm^{-1} for CrH and 1650.9 and 1614.5 cm^{-1} for CrH$_2$, and the Cr−D stretching frequencies with 1158.7 cm^{-1} for CrD and 1166.8 and 1188.9 cm^{-1} for CrD$_2$.[23] Binary chromium hydride absorptions are not observed in the present infrared spectra. The product hydrogen stretching frequencies also show no shift in the CH$_2$CD$_2$ spectra, indicating that the primary product contains a Cr−H group, whose stretching mode is not perturbed by neighboring C−H stretching mode. This strongly suggests that the **i** absorptions arise from CrH−CHCH$_2$. The **i** absorption at 568.0 cm^{-1} has its ^{13}C counterpart at 557.1 cm^{-1} (12/13 ratio of 1.020) and is assigned to the C−Cr stretching mode on the basis of the sizable ^{13}C shift without observation of the D counterpart.

The **a** absorption at 861.5 cm^{-1} has its ^{13}C counterpart at 851.4 cm^{-1} (12/13 ratio of 1.012) and is assigned to the B_2 CH$_2$ wagging mode of the π-complex (Cr−CH$_2$CH$_2$), which is expected to be strongest among the generally weak bands of this product as shown in Table 9. This unusually large C-13 shift (10.1 cm^{-1}) of a mode at this frequency requires an out-of-plane deformation of an ethylene-like skeleton. (In contrast, the bending mode computed at 898.4 cm^{-1} for the insertion product has a calculated 7.3 cm^{-1} C-13 shift.) The weak absorption at 711.3 cm^{-1} in a congested area with the precursor absorptions (not shown) is designated to the D counterpart. No other **a** absorptions are observed, due to their low absorption intensities as shown in Table 9, and accordingly this identification, although straightforward, is tentative. Such **a** complex absorptions are observed only in the Cr spectra, and B3LYP calculations also show that the metallacyclopropane complex is most stable among the plausible products: Cr−C$_2$H$_4$(Q), CrH−CHCH$_2$(Q), and CrH$_2$−C$_2$H$_2$(T) are computed to be 0.4, 4.7, and 32 kcal/mol higher than the reactants (^{7}Cr + C$_2$H$_4$). The dihydrido complex (CrH$_2$−C$_2$H$_2$) is not identified from the matrix infrared spectra, most probably due to its considerably higher energy. The DFT calculated frequencies of the dihydrido Cr complex are listed in Table S3.

Primary Products. Figure 8 shows the energies of the most plausible group 6 metal products relative to the reactants. The metallacyclopropane and insertion complexes have a quintet ground state, whereas the dihydrido product has a triplet ground state. WH$_2$−C$_2$H$_2$ is the most stable among the plausible W products, and the insertion and metallacyclopropane complexes are energetically comparable to one another. Because the dihydrido and insertion products are identified in the matrix spectra, it is expected that the metallacyclopropane complex is also a primary product from reactions of W with ethylene isotopomers.

In the Mo system, the metallacyclopropane and dihydrido complexes are the most stable, while the absorptions of the dihydrido complex and less stable insertion complexes are observed. Tables S1 and S2 show the DFT vibrational characteristics for the W and Mo metallacyclopropane. Notice that the vibrational bands of the metallacyclopropane complexes are all predicted to be very weak, and, therefore, they are difficult to identify unless the product yield is high enough. In the Cr system, the metallacyclopropane complex is the single most stable species, and as a result, more Cr metallacyclopropane is probably produced, resulting in observation of the B_2 CH$_2$ wagging absorption. The present results are also in agreement with the observed general trend that higher oxidation-state complexes become more stable on going down the group column.[3,12,13]

Our investigations with CH$_2$CD$_2$ demonstrate clearly that the dihydrido complex is formed by β-hydrogen transfer in the insertion complex because all three possible mixed H/D isotopic complexes are formed, but the MHD−CHCD isotopopmer is dominant (Figures 3 and 6). The insertion complex structures (Figure 9) show that β and α hydrogen atoms are about the same distance from the metal center, and it appears from the spectra that β hydrogen transfer on visible light excitation of the insertion complex is the favored process, as discussed for the group 5 metal and ethylene system.[13]

The clear absence of isolated binary group 6 metal hydride absorptions in the product infrared spectra is unique among the early transition-metal systems,[4−7,9−13] suggesting that H$_2$-elimination of ethylene by group 6 metals is a slower process. The released H$_2$ from reactions of the metal atoms with ethylene

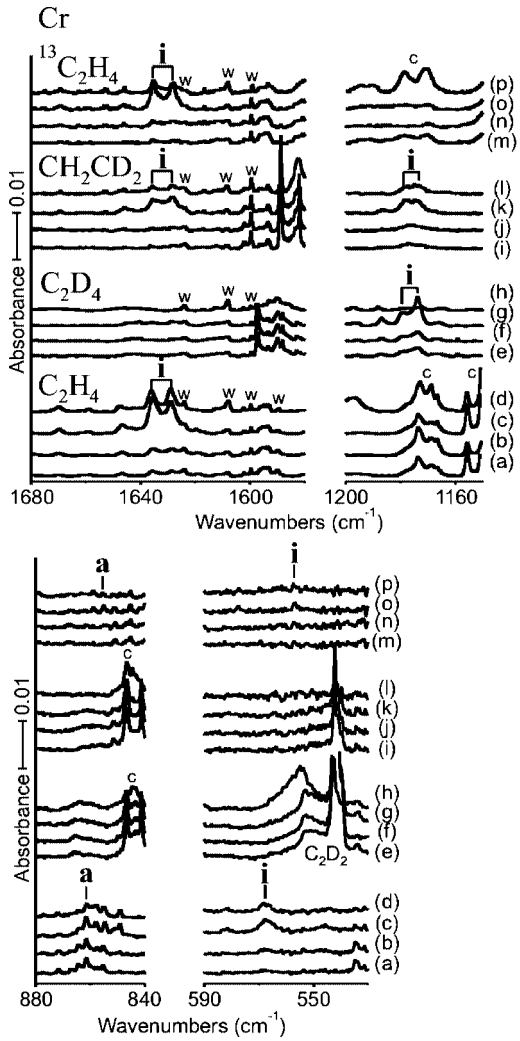

Figure 7. IR spectra in the regions of 1680−1580, 1200−1150, 880−840, and 590−530 cm^{-1} for laser-ablated Cr atoms codeposited with ethylene isotopomers in excess argon at 10 K and their variation. (a) Cr + 0.5% C_2H_4 in Ar codeposited for 1 h. (b) As (a) after photolysis with $\lambda > 420$ nm. (c) As (b) after photolysis with $240 < \lambda < 380$ nm. (d) As (c) after annealing to 36 K. (e) Cr + 0.5% C_2D_4 in Ar codeposited for 1 h. (f) As (e) after photolysis with $\lambda > 420$ nm. (g) As (f) after photolysis with $240 < \lambda < 380$ nm. (h) As (g) after annealing to 40 K. (i) Cr + 0.5% CH_2CD_2 in Ar codeposited for 1 h. (j) As (i) after photolysis with $\lambda > 420$ nm. (k) As (j) after photolysis with $240 < \lambda < 380$ nm. (l) As (k) after annealing to 36 K. (m) Cr + 0.5% $^{13}C_2H_4$ in Ar codeposited for 1 h. (n) As (m) after photolysis with $\lambda > 420$ nm. (o) As (n) after photolysis with $240 < \lambda < 380$ nm. (p) As (o) after annealing to 36 K. **i** and **d** denote the product absorption groups. c and w denote common and water residual absorptions.

TABLE 7: Frequencies of Product Absorptions Observed from Reactions of Ethylene with Cr in Excess Argon[a]

	C_2H_4	C_2D_4	$^{13}C_2H_4$	CH_2CD_2	description
a	861.5	711.3	851.4		B_2 CH_2 wag
i	1635.5, 1628.8	1179.6, 1173.8	1635.3, 1628.4	1635.2, 1628.4, 1178.6, 1173.6	Cr−H str.
	568.0		557.1		C−Cr str.

[a] All frequencies are in cm^{-1}. Description gives major coordinate. **a** and **i** stand for metallacyclopropane and insertion products, respectively.

would form metal hydrides during codeposition and the process of photolysis as reported in the previous matrix infrared investigations of groups 4 and 5.[12,13] The previous reaction dynamics studies suggest that H_2-elimination occurs from the dihydrido complex, leaving a metal−acetylene complex.[4−7,9] Figure 8 also shows that [H_2 + W−C_2H_2(Q)] is only 7 kcal/mol more stable than the reactants and 46 kcal/mol higher than WH_2−C_2H_2(T). The combination [H_2 + Mo−C_2H_2(Q)] is 13 and 28 kcal/mol higher than the reactants and MoH_2−C_2H_2(T).

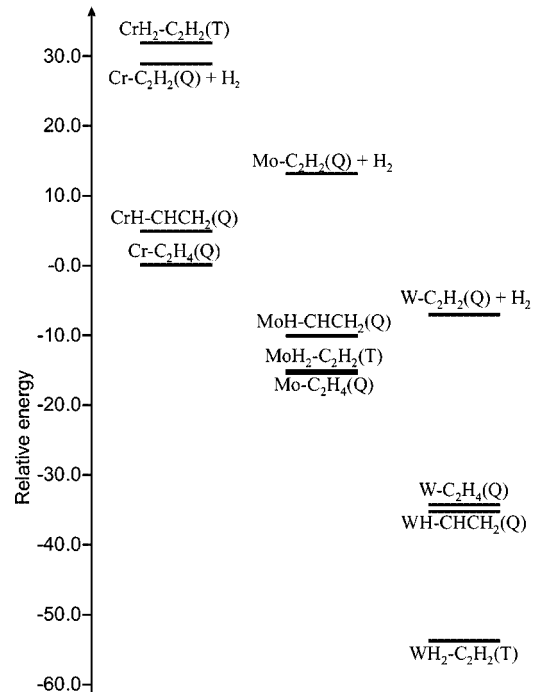

Figure 8. Energies of the most stable products from reactions of group 6 metals with ethylene relative to the reactants, which is zero on each energy scale. Notice that the W complexes are more stable than the corresponding Cr and Mo complexes, which is consistent with the relatively most stable product absorptions observed in the W spectra (see text). T denotes triplet and Q quintet electronic states.

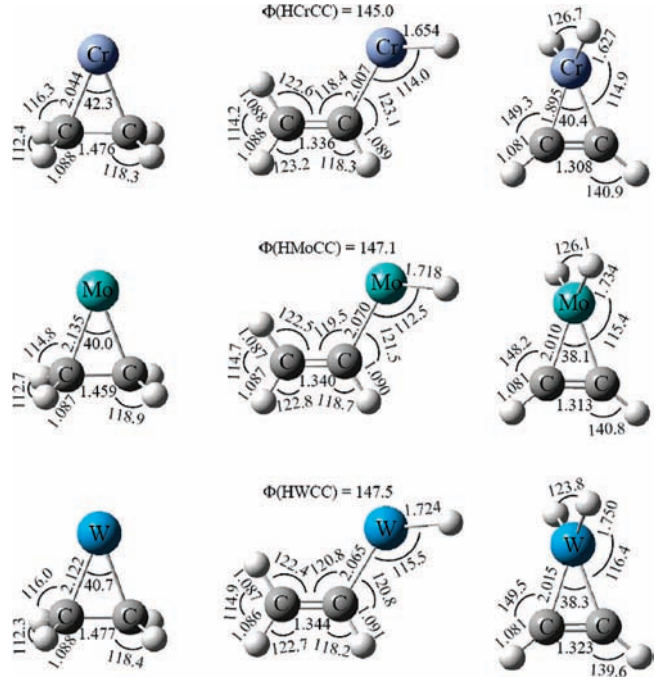

Figure 9. Product structures for reactions of group 6 metals and ethylene. The metallacyclopropane, insertion, and dihydrido products in the ground quintet, quintet, and triplet states have C_{2v}, C_1, and C_{2v} structures, respectively. The bond lengths and angles are in angstroms and degrees, and the HMCC dihedral angles for the insertion complexes are also shown.

TABLE 8: Observed and Calculated Frequencies of the Fundamental Bands of $CrH-CHCH_2$ in Its Ground ^5A State[a]

	$CrH-CHCH_2$				$CrD-CDCD_2$				$CrH-^{13}CH^{13}CH_2$			
description	obs.[b]	BPW91[c]	B3LYP[d]	int.[d]	obs.[b]	BPW91[c]	B3LYP[d]	int.[d]	obs.[b]	BPW91[c]	B3LYP[d]	int.[d]
CH_2 as. str.		3067.2	3126.9	25		2279.9	2325.6	8		3055.3	3114.5	26
C−H str.		3040.4	3088.0	3		2249.1	2283.6	1		3030.6	3078.3	3
CH_2 s. str.		3000.1	3062.4	24		2180.9	2226.4	10		2994.6	3056.7	24
Cr−H str.	1635.5	1670.9	1670.7	239	1173.8	1193.4	1193.3	128	1635.2	1670.8	1670.5	241
C═C str.		1541.5	1598.7	5		1462.6	1514.6	7		1502.5	1559.5	3
CH_2 scis.		1370.8	1420.0	11		1026.5	1067.4	7		1350.3	1397.7	10
HCCH IP s. bend		1189.1	1243.5	25		965.7	1002.0	7		1173.8	1228.3	26
HCCH OOP bend		973.0	1028.5	14		735.8	782.4	2		970.0	1025.2	15
CH_2 g		903.4	959.0	31		706.4	744.2	27		897.4	945.8	25
HCCH IP as. bend		898.4	951.1	15		656.1	694.1	7		891.1	950.4	19
C−Cr str.	568.0	552.7	554.5	119		493.6	492.0	60	557.1	543.2	545.8	123
CCrH bend		439.2	445.2	31		340.4	349.0	29		434.6	439.6	27
CH_2 twist		329.6	339.4	33		252.1	260.6	22		327.0	336.6	31
CCCr bend		117.0	119.5	25		90.6	104.4	19		116.1	117.0	25
CrH OOP bend		73.9	82.7	100		61.5	61.2	51		72.6	82.3	100

[a] Frequencies and intensities are in cm^{-1} and km/mol. [b] Observed in an argon matrix. [c] Frequencies computed with BPW91/6-311++G(3df,3pd). [d] Frequencies and intensities computed with B3LYP/6-311++G(3df, 3pd). $CrH-CHCH_2$ has a C_1 structure.

TABLE 9: Observed and Calculated Frequencies of the Fundamental Bands of $Cr-C_2H_4$ in Its Ground $^5B_2$ State[a]

	$Cr-C_2H_4$				$Cr-C_2D_4$				$Cr-^{13}C_2H_4$			
description	obs.[b]	BPW91[c]	B3LYP[d]	int.[d]	obs.[b]	BPW91[c]	B3LYP[d]	int.[d]	obs.[b]	BPW91[c]	B3LYP[d]	int.[d]
A_1 CH str.		2997.8	3061.6	20		2181.7	2227.3	7		2992.0	3055.8	21
A_1 CH_2 scis.		1415.0	1462.0	0		1157.9	1175.4	5		1405.5	1453.1	0
A_1 C═C str		1052.2	1049.4	15		882.0	893.1	11		1021.8	1019.5	13
A_1 CH_2 wag.		825.3	838.9	5		634.7	635.	1		819.6	832.8	6
A_1 CrC_2 str.		479.5	435.8	1		453.1	419.0	2		468.7	425.6	1
A_2 CH str.		3055.0	3115.2	0		2272.3	2317.6	0		3043.1	3103.0	0
A_2 CH_2 rock		1160.6	1200.6	0		910.7	941.4	0		1149.1	1188.7	0
A_2 CH_2 twist		539.2	546.1	0		390.8	395.6	0		537.7	544.6	0
B_1 CH str.		3078.3	3139.4	21		2285.3	2330.8	7		3066.3	3127.2	22
B_1 CH_2 rock		764.4	797.4	1		545.6	568.7	0		763.9	796.9	1
B_1 CH_2 twist		530.7	537.2	26		393.1	398.2	18		528.8	535.2	25
B_2 CH str.		2989.9	3051.6	31		2161.1	2205.9	12		2985.0	3046.5	31
B_2 CH_2 scis.		1380.6	1428.0	0		1019.6	1054.5	2		1375.7	1422.9	0
B_2 CH_2 wag.	861.5	862.3	886.8	48	711.3	712.3	724.6	21	851.4	851.5	876.4	48
B_2 CrC_2 str.		459.2	444.0	22		409.3	400.0	24		446.5	431.4	20

[a] Frequencies and intensities are in cm^{-1} and km/mol. [b] Observed in an argon matrix. [c] Frequencies computed with BPW91/6-311++G(3df,3pd). [d] Frequencies and intensities computed with B3LYP/6-311++G(3df, 3pd). $Cr-C_2H_4$ has a C_{2v} structure.

$[H_2 + Cr-C_2H_2(Q)]$ is 29.0 and kcal/mol higher than the reactants and 3 kcal/mol lower than $CrH_2-C_2H_2(T)$, which is not identified. Therefore, H_2-elimination by group 6 metals is apparently energetically less favored than that by other early transition metals.[5−7,9,13]

Product Structures. Figure 9 illustrates the most plausible product structures from reactions of group 6 metals and ethylene. The metallacyclopropane, insertion, and dihydrido complexes have C_{2v}, C_1, and C_{2v} structures. In the insertion complex, the metal, two C, and three H atoms form a near planar structure, and the remaining H atom bonded to the metal atom is out of the near planar structure. The carbon−metal and carbon−carbon bond lengths decrease in the order of metallacyclopropane, insertion, and dihydrido complexes. The shorter C−C bond of the insertion complex than the metallacyclopropane reflects the fact that the bond in the metallacyclopropane complex is essentially a single C−C bond. The higher s character in the C−M bond in the insertion complex, therefore, leads to the shorter bond relative to those in the metallacyclopropane. For instance, the natural bond orbital (NBO)[15,24] s characters in the C−W bonds in insertion and metallacyclopropane complexes are 28.4% and 14.5%.

The shortest C−C and C−M bonds in the dihydrido complex also draw attention. The metal atom in a higher oxidation state tends to form a stronger bond.[21−23] In addition, stronger back-donation to the π^* orbital is expected to occur in the dihydrido complex, which further strengthens the C−M bonds. Interestingly enough, the NBO occupancy of the C−C π^* orbital for the dihydrido complex is lower than that for the insertion complex, for example, 0.0463 and 0.0364 for $MoH-CHCH_2$ and $MoH_2-C_2H_2$. This evidently leads to the shorter C−C bond. In contrast, the NBO occupancy of the C−M σ^* orbital for the dihydrido complex is higher than that for the insertion complex, for example, 0.0495 and 0.0233 for $MoH_2-C_2H_2$ and $MoH-CHCH_2$. Obviously further investigation is needed, and we leave more details of these interesting interactions to future theoretical studies.

The carbon−metal bond lengths of the metallacyclopropane and insertion complexes first increase from Cr to Mo, but then decrease from Mo to W. Similarly the carbon−metal bond length of the dihydrido complex increases substantially (0.115 Å) from Cr to Mo, but it increases only 0.005 Å from Mo to W. The observed MC_2 stretching frequency also increases from 611.8 cm^{-1} for $MoH_2-C_2H_2$ to 644.7 cm^{-1} for $WH_2-C_2H_2$. These variations are evidence for the larger relativistic bond-length contraction for the third-row transition metal predicted by Pyykko et al.[25] The C−M bonds of group 4 metal−acetylene

complexes also show a similar variation: the C−M bond lengths are 1.962, 2.054, and 2.044 Å on going down the group 4 column.[12]

Conclusions

Reactions of laser-ablated group 6 metals with ethylene have been carried out, and the primary products are identified in the matrix spectra on the basis of their vibrational characteristics. The insertion and dihydrido complexes are identified from reactions of W and Mo with ethylene isotopomers, while the absorptions from the insertion and metallacyclopropane complexes are observed in the Cr spectra. The DFT frequency calculations reproduce the observed spectra: the high oxidation-state dihydrido complex, $MH_2-C_2H_2$, becomes more stable relative to the other plausible products on going down the column, consistent with the previous studies of small metal complexes.[3,4,12,13] Our experiments with CH_2CD_2 demonstrate that the dihydrido complex is formed by β-hydrogen transfer within the insertion complex because the MHD−CHCD isotopic product dominates the spectrum.

The Cr dihydrido complex is too high in energy to form, whereas the W and Mo metallacyclopropane complexes are probably generated, but their absorptions are too weak to be observed. Unlike the cases of group 4 and 5 metals, binary metal hydride absorptions are not observed,[12,13,21−23] suggesting that H_2-elimination of ethylene by group 6 metals does not occur readily, consistent with the lower gas-phase reactivity reported previously.[11] The H_2-elimination step from the W and Mo dihydrido complexes ($MH_2-C_2H_2$) is believed to be slow, whereas the Cr dihydrido complex is not easily formed.

Acknowledgment. We gratefully acknowledge financial support from the National Science Foundation (U.S.) Grant CHE 03-52487 to L.A., and support from the Korea Institute of Science and Technology Information (KISTI) by Grant No. KSC-2006-S00-2014.

Supporting Information Available: Tables of calculated product frequencies. This material is available free of charge via the Internet at http://pubs.acs.org.

References and Notes

(1) (a) Hall, C.; Perutz, R. N. *Chem. Rev.* **1996**, *96*, 3125.

(2) (a) Campos, K. R. *Chem. Soc. Rev.* **2007**, *36*, 1069. (b) Díaz-Requejo, M. M.; Belderrain, T. R.; Nicasio, M. C.; Pérez, P. J. *Dalton Trans.* **2006**, 5559.

(3) Andrews, L.; Cho, H.-G. *Organometallics* **2006**, *25*, 4040, and references therein (review article).

(4) Lee, Y. K.; Manceron, L.; Papai, I. *J. Phys. Chem. A* **1997**, *101*, 9650.

(5) (a) Yi, S. S.; Blomberg, M. R. A.; Siegbahn, P. E. M.; Weisshaar, J. C. *J. Phys. Chem. A* **1998**, 102. (b) Reichert, E. L.; Yi, S. S.; Weisshaar, J. C. *Int. J. Mass Spectrom.* **2000**, *196*, 55. (c) Wen, Y.; Poremski, M.; Ferrett, T. A.; Weisshaar, J. C. *J. Phys. Chem. A* **1998**, *102*, 8362. (d) Carroll, J. J.; Haug, K. L.; Weisshaar, J. C. *J. Am. Chem. Soc.* **1993**, *115*, 6962. (e) Poremski, M.; Weisshaar, J. C. *J. Phys. Chem. A* **2000**, *104*, 1524. (Zr + hydrocarbons).

(6) (a) Hinrichs, R. Z.; Schroden, J. J.; Davis, H. F. *J. Am. Chem. Soc.* **2003**, *125*, 860. (b) Schroden, J. J.; Wang, C. C.; Davis, H. F. *J. Phys. Chem. A* **2003**, *107*, 9295. (c) Porembski, M.; Weisshaar, J. C. *J. Phys. Chem. A* **2001**, *105*, 6655. (d) Stauffer, H. U.; Hinrichs, R. Z.; Schroden, J. J.; Davis, H. F. *J. Phys. Chem. A* **2000**, *104*, 1107. (e) Hinrichs, R. Z.; Schroden, J. J.; Davis, H. F. *J. Phys. Chem. A* **2003**, *107*, 9284 (Y + hydrocarbons).

(7) (a) Willis, P. A.; Stauffer, H. U.; Hinrichs, R. Z.; Davis, H. F. *J. Phys. Chem. A* **1999**, *103*, 3706. (b) Rivalta, I.; Russo, N.; Sicilia, E. *J. Mol. Struct. (THEOCHEM)* **2006**, *762*, 25 (Nb + C_2H_4).

(8) (a) Parnis, J. M. P.; Lafleur, R. D.; Rayner, D. M. *J. Phys. Chem.* **1995**, *99*, 673. (b) Thompson, M. G. K.; Parnis, J. M. *J. Phys. Chem. A* **2005**, *109*, 9465.

(9) Poremski, M.; Weisshaar, J. C. *J. Phys. Chem. A* **2001**, *105*, 4851 (Zr + C_2H_4 reaction path).

(10) (a) Siegbahn, P. E. M.; Blomberg, M. R. A.; Svensson, M. *J. Am. Chem. Soc.* **1993**, *115*, 1952. (b) Blomberg, M. R. A.; Siegbahn, P. E. M.; Svensson, M. *J. Phys. Chem.* **1992**, *96*, 9794. (c) Blomberg, M. R. A.; Siegbahn, P. E. M.; Yi, S. S.; Noll, R. J.; Weisshaar, J. C. *J. Phys. Chem. A* **1999**, *103*, 7254.

(11) (a) Carroll, J. J.; Haug, K. L.; Weisshaar, J. C.; Blomberg, M. R. A.; Siegbahn, P. E. M.; Svensson, M. *J. Phys. Chem.* **1995**, *99*, 13955. (b) Carroll, J. J.; Weisshaar, J. C. *J. Phys. Chem.* **1996**, *100*, 12355.

(12) (a) Cho, H.-G.; Andrews, L. *J. Phys. Chem. A* **2004**, *108*, 3965 (Zr + C_2H_4). (b) Cho, H.-G.; Andrews, L. *J. Phys. Chem. A* **2004**, *108*, 10441 (Ti and Hf + C_2H_4).

(13) Cho, H.-G.; Andrews, L. *J. Phys. Chem. A* **2007**, *111*, 5201 (group 5 + C_2H_4).

(14) (a) Andrews, L.; Citra, A. *Chem. Rev.* **2002**, *102*, 885, and references therein. (b) Andrews, L. *Chem. Soc. Rev.* **2004**, *33*, 123, and references therein.

(15) Kudin, K. N.; Burant, J. C.; Millam, J. M.; Iyengar, S. S.; Tomasi, J.; Barone, V.; Mennucci, B.; Cossi, M.; Scalmani, G.; Rega, N.; Petersson, G. A.; Nakatsuji, H.; Hada, M.; Ehara, M.; Toyota, K.; Fukuda, R.; Hasegawa, J.; Ishida, M.; Nakajima, T.; Honda, Y.; Kitao, O.; Nakai, H.; Klene, M.; Li, X.; Knox, J. E.; Hratchian, H. P.; Cross, J. B.; Adamo, C.; Jaramillo, J.; Gomperts, R.; Stratmann, R. E.; Yazyev, O.; Austin, A. J.; Cammi, R.; Pomelli, C.; Ochterski, J. W.; Ayala, P. Y.; Morokuma, K.; Voth, G. A.; Salvador, P.; Dannenberg, J. J.; Zakrzewski, V. G.; Dapprich, S.; Daniels, A. D.; Strain, M. C.; Farkas, O.; Malick, D. K.; Rabuck, A. D.; Raghavachari, K.; Foresman, J. B.; Ortiz, J. V.; Cui, Q.; Baboul, A. G.; Clifford, S.; Cioslowski, J.; Stefanov, B. B.; Liu, G.; Liashenko, A.; Piskorz, P.; Komaromi, I.; Martin, R. L.; Fox, D. J.; Keith, T.; Al-Laham, M. A.; Peng, C. Y.; Nanayakkara, A.; Challacombe, M.; Gill, P. M. W.; Johnson, B.; Chen, W.; Wong, M. W.; Gonzalez, C.; Pople, J. A. *Gaussian 03*, revision B.04; Gaussian, Inc.: Pittsburgh, PA, 2003.

(16) (a) Becke, A. D. *J. Chem. Phys.* **1993**, *98*, 5648. (b) Lee, C.; Yang, Y.; Parr, R. G. *Phys. Rev. B* **1988**, *37*, 785.

(17) Raghavachari, K.; Trucks, G. W. *J. Chem. Phys.* **1989**, *91*, 1062.

(18) Andrae, D.; Haeussermann, U.; Dolg, M.; Stoll, H.; Preuss, H. *Theor. Chim. Acta* **1990**, *77*, 123.

(19) Burke, K.; Perdew, J. P.; Wang, Y. In *Electronic Density Functional Theory: Recent Progress and New Directions*; Dobson, J. F., Vignale, G., Das, M. P., Eds.; Plenum: New York, 1998.

(20) (a) Scott, A. P.; Radom, L. *J. Phys. Chem.* **1996**, *100*, 16502. (b) Andersson, M. P.; Uvdal, P. L. *J. Phys. Chem. A* **2005**, *109*, 3937.

(21) Wang, X.; Andrews, L. *J. Phys. Chem. A* **2002**, *106*, 6720.

(22) Wang, X.; Andrews, L. *J. Phys. Chem. A* **2005**, *109*, 9021.

(23) Wang, X.; Andrews, L. *J. Phys. Chem. A* **2003**, *107*, 570.

(24) (a) Reed, A. E.; Weinstock, R. B.; Weinhold, F. *J. Chem. Phys.* **1985**, *83*, 735. (b) Reed, A. E.; Curtiss, L. A.; Weinhold, F. *Chem. Rev.* **1988**, *88*, 899.

(25) (a) Pyykko, P.; Desclaux, J. P. *Chem. Phys. Lett.* **1977**, *50*, 503. (b) Pyykko, P.; Snijders, J. G.; Baerends, E. J. *Chem. Phys. Lett.* **1981**, *83*, 432. (c) Ziegler, T.; Snijders, J. G.; Baerends, E. J. *J. Chem. Phys.* **1981**, *74*, 1271. (d) Pyykko, P. *Chem. Rev.* **1988**, *88*, 563.

JP806110H